Medical Engineering and Physics 103 (2022) 103786

Contents lists available at ScienceDirect

Medical Engineering and Physics

journal homepage: www.elsevier.com/locate/medengphy

Selection of animal bone surrogate samples for orthopaedic screw testing based on human radius CT-derived bone morphology☆

J.D. Silva-Henao [*,a,b], A. Synek [b], D.H. Pahr [a,b], A.G. Reisinger [a,b]

[a] Karl Landsteiner University of Health Sciences, Department of Anatomy and Biomechanics, Division Biomechanics, Dr. Karl-Dorrek-strae 30, 3500, Krems, Austria
[b] Institute of Lightweight Design and Structural Biomechanics, Technische Universität Wien, Vienna, Austria

ARTICLE INFO

Keywords:
Bone
Bone morphology
Sample selection
Computer tomography
Data visualization
Orthopaedic implants

ABSTRACT

Animal bones are commonly used to test the mechanical competence of bone screws since they are easier to obtain compared to human bones. Nevertheless, selecting an appropriate animal sample that correctly represents the human bone architecture where the screw is implanted is frequently overlooked. This study presents a protocol for bone sample selection for screw mechanical testing based on a characterization of the local CT-derived bone morphology. For this, 36 human radii were used to quantify the local peri-implant bone morphology of 360 osteosynthesis screws, 10 per bone, whose implantation site and depth were fully known. A cylindrical volume of interest was created along the screw path and used to measure the local morphology. With this, 10 average peri-implant bone morphologies were defined. Additionally, two animal models, pig, and sheep, were selected and used as potential sample sources. From each model, six bones were selected for analysis. Based on a surface mesh of each bone a computational algorithm was created to automatically extract cylindrical probes in several locations from which the local bone morphometry was calculated. A multi-parametric bone similarity score was developed and used to compare the local morphology of each animal bone to that of the human average peri-implant bone morphology. The score was then mapped to the surface of the bone thus allowing to visually identify regions on the animal bone with human-like bone morphology. By using this methodology, the use of human bones can be avoided since samples with human-like bone morphologies can be found on animal bones. This is not only useful in cases where strict ethical constrains must be fulfilled, but also in studies where the relationship between morphology and screw competence is to be studied, something that is hard to replicate with commercially available synthetic alternatives.

1. Introduction

Due to the increasing rate of bone fractures, particularly in older population prone to bone degenerative diseases such as osteoporosis, the use of orthopaedic implants is on the rise. A wide number of orthopaedic implants are hold in place by metal screws which are prone to complications including, but not limited to, screw cut-out [1], screw loosening [2–4] and screw breakage [2,3,5] which require costly and inconvenient revision surgeries. Furthermore, several studies have presented the relationship between screw purchase and/or holding power and the underlying bone architecture. More specifically, peri-implant bone volume [6], bone volume fraction [7], bone mineral density [8] and cortical thickness [9] have been demonstrated to be good predictors of implant stability. What most studies have in common is the use of human bone, either whole or harvested biopsies, with most of these studies focused on the proximal humerus, femoral head, spine, and tibia. The reasons for testing orthopaedic screws in human bone are clear, there is the possibility of placing the implants in the real implantation site and subject them to real anatomical loading scenarios. Despite this, testing human bones has significant drawbacks such as limited number of suitable specimens [10] with high inter-subject variation and limited demographic representation [11] since most bone donors are older and often diseased patients; this in addition to the need of long and very strict ethic revisions in basically every case.

Commercially available synthetic bone models, frequently made of expanded PU foam, offer a viable alternative for testing orthopaedic implants since they accurately represent the elastic mechanical properties of bone [12,13]. Previous studies have used synthetic bone

☆ word count, excluding references and captions: **5535 words**

* Corresponding author.
E-mail address: juan.silva@kl.ac.at (J.D. Silva-Henao).

https://doi.org/10.1016/j.medengphy.2022.103786
Received 6 August 2021; Received in revised form 26 January 2022; Accepted 1 March 2022
Available online 2 March 2022

analogues for testing different screw thread designs [14,15], materials [16] or type [17], i.e. cortical vs. trabecular screw. However, as pointed out in previous works [13,18] common synthetic bone analogues do not accurately represent the failure and plastic mechanical properties of bone in addition to the variability present in human bone structures [19], which means that they are not ideal for testing the influence of the underlying bone morphology on the mechanical competence of an implanted screw. additionally, these materials might not be available everywhere which makes them expensive and time consuming due to lengthy shipping times and fees.

Animal bone samples, which could compensate the inherent drawbacks of testing in human bone samples and synthetic bone analogues, have been used in the past for screw and implant related research with general success [20]. Nevertheless, to the best of the authors knowledge there is not a defined methodology or protocol for sample selection.

As a general rule, the size, shape and number of implants (understood hereon and for the purpose of this study, as screw shaped objects) determines the animal model that should be used [21], meaning that the chosen implant must be tested in an animal bone with a size comparable to its human counterpart [22]. Because of this, animal bones and animal bone biopsies are selected mostly based on anatomical correspondence, that is for example, pedicle screws implanted in calf, sheep or pig spines [23–27] and dental implants placed in ovine, porcine and canine mandible [28–32]. However, is not uncommon to find "odd" combinations such as dental screws implanted in bovine tibia [33] and porcine ribs [34,35] when certain morphological characteristics are desired, such as variable cortical thickness or specific bone volume fraction respectively, or dental screws implanted in sheep spine [6] with sample selection based purely on bone availability. The point here is not to question the validity of the aforementioned studies, since it has been proved that animal bone samples have comparable mechanical properties to human bones [36–38], but rather point out to the fact that, as it has been done by several authors before [21,39–41], there is an increasing need for "gold standard" method for animal surrogate sample selection for orthopaedic implant testing.

Recent efforts have successfully determined the similarity between bone tissue samples and synthetic materials, such as bio-ceramic scaffolds, by quantifying the structural parameters (for example porosity or degree of anisotropy) of both samples, biological and synthetic, and defining a multi-parametric similarity score which rates how close both structures are to each other [42–44]. Furthermore, this same approach has been used to compare the tactile properties of liver tissue and soft polymeric samples [45] suggesting that this same approach can be successfully adapted to a different set of descriptive parameters, for example mechanical properties.

At an organ level, bones present regional morphological variations [46] which can complicate the definition of an ideal bone sample source for screw mechanical testing. It is common that a single screw type is used to hold in place an osteosynthesis plate system that covers a large portion of the bone, as it can be seen in [47,48], meaning that a single screw is implanted in different types of bone architectures. Because of this, a similar approach to that presented in [48] where a cylindrical bone segment along the screw path is isolated and used to determine the peri-implant bone morphology can be used to define the "average" peri-implant bone morphology in which a certain type of screw is implanted. Furthermore, local bone morphometry from an animal bone can be recorded in several locations all over the bone and compared to the aforementioned average peri-implant bone morphology using a similarity score close to those presented in [42] or [45] which would in turn point to an ideal sample harvesting location on an animal bone.

With this in mind, the aim of this study is the development and implementation of a methodology for surrogate sample selection from an animal bones which can be used to test orthopaedic implants. In other words, the proposed methodology provides a path for identifying sample harvesting locations on animal bones which best represent the local bone morphometry in which a certain screw type is implanted, for example, a human distal radius osteosynthesis screw. This is something of great importance when assessing the mechanical competence of orthopaedic screws and the effect of the underlying bone morphology but has not yet been thoroughly studied to the best of the authors knowledge. In the future, this could be of considerable advantage for biomechanical studies, especially if human tissue is hardly available for science.

2. Materials and methods

A graphical overview of the methodology followed on the this study is presented in figure 1 and will be thoroughly explained in the following sections.

In short, local CT-derived bone morphometric values (CT-MV) were calculated from 36 human radii [47,49] on which 10 distal radius osteosynthesis screws (360 screws in total) were implanted. The implantation sites, orientations and depths of every screw was fully known. The local peri-implant CT-MVs were calculated from a cylindrical volume of interest along the screw path which was extracted from a computed tomography (CT) image taken prior to screw implantation and used to define ten average peri-implant CT-MVs, one for each implantation site. Simultaneously, a set of 12 animal bones taken from both pig and sheep (six each) were analysed using an in-house built computational algorithm in which a large number of locations on the surface of each bone were probed and the local CT-MVs were recorded. These values were compared to the ten average peri-implant human bone CT-MVs by means of a multi parametric bone similarity score (BoSS) based on that presented in [42] but using the parameters suggested in [50] which are widely considered standard bone micro structural measurements. The resulting BoSS was projected as a colour map to the surface of each animal bone. In order to better interpret these results a range of human BoSS values was determined by comparing each peri-implant bone segment to its respective average bone segment and used to define a threshold of human-like BoSS values. Finally, the BoSS colour maps were remapped to reflect the established human-like categories and, thus, simplifying the identification of optimal regions for sample harvesting.

2.1. Human bone analysis

Detailed information about human bone provenance and handling can be found in [47] and [49], studies from where the CT scans were procured. In these studies, all human bones were scanned using a HR-pQCT device (XtremeCT, ScancoMedicalAG, Brttisellen, Switzerland) with a voxel size of 0.082 mm a tube potential of 60 kVp and a current of 900 μA. Afterwards, ten 2.5 distal radius locking screws were used to secure a distal radius volar plate implant making the implantation position and depth (x-y-z coordinates of the entry and end points) of each screw fully known. Screw implantation was done using the manufactures drill guide block thus guaranteeing a consistent implantation angle in each site.

With this information (implantation coordinates), a peri-implant bone segment corresponding to a cylinder mask with a 4 mm diameter, shown in figure 2, was created around every screw implantation site from which the local bone MVs were calculated. all image processing was done using python scripts made for medtool (Medtool 4.3, Dr. Pahr Ingenieurs e.U., Pfaffstätten, Austria). The diameter of the VOI was selected based in [33] and [48] which was kept constant for both animal and human specimens. The length was set to coincide with the implantation depth of each screw.

This process was repeated for 36 human radii yielding a total of 360 peri-implant bone segments, ten per each implantation site marked in the plate (figure 2) from 1 to 10. For each peri-implant bone segment the following MVs were recorded:

- Ct.Th.: Cortical thickness [mm]

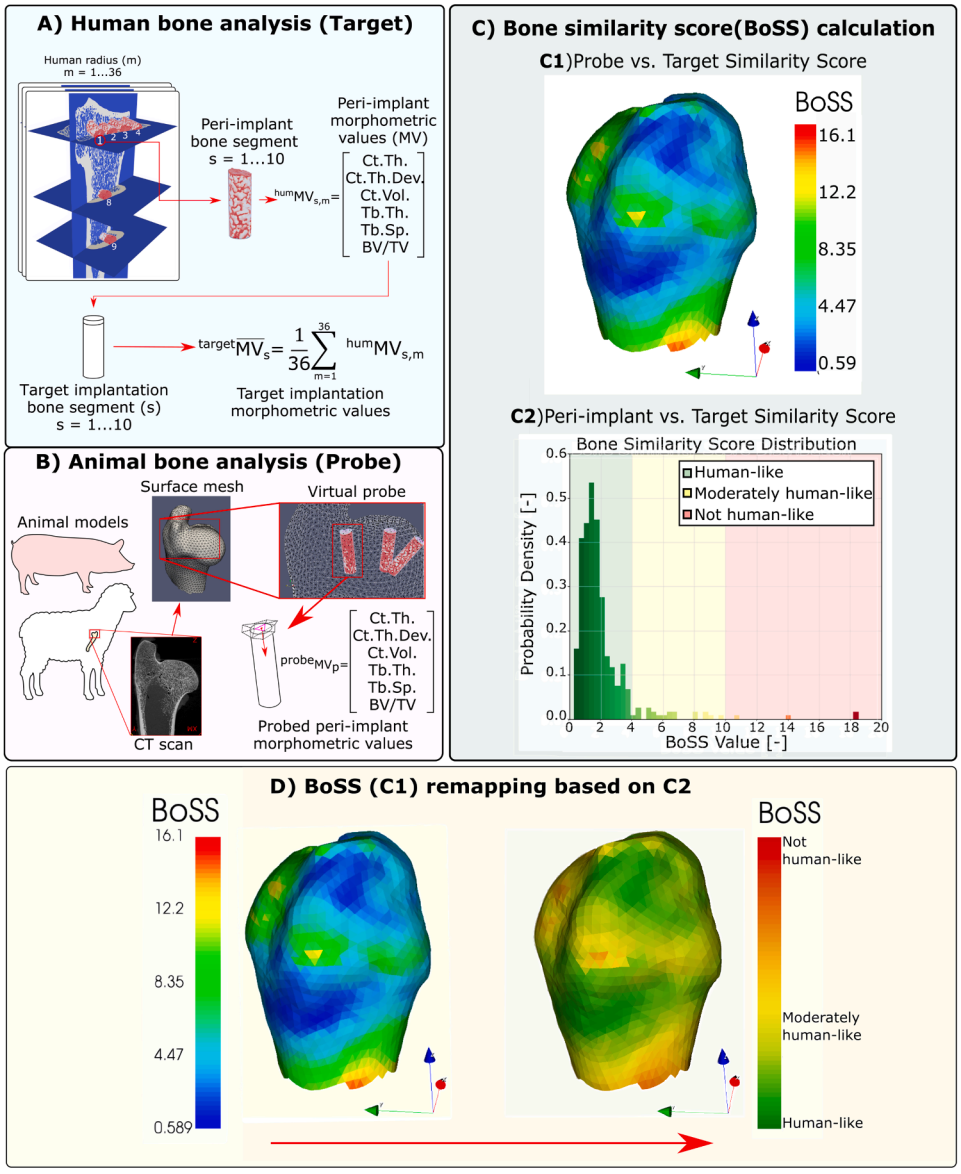

Fig. 1. Methodology overview.(A) Measuring the CT-derived peri-implant morphometric values from human bones and creating of target average bone segment at a specific screw location. (B) Virtual probing and recording of local CT-derived morphometric values on multiple location on animal bones. (C) Calculation of bone similarity score between target bone segments and animal probes projected to the bone surface (C1, done for each target bone segment) as well as target and peri-implant samples (C2). (D) Human-like recolouring of BoSS values based on C2 for sample harvesting region identification.

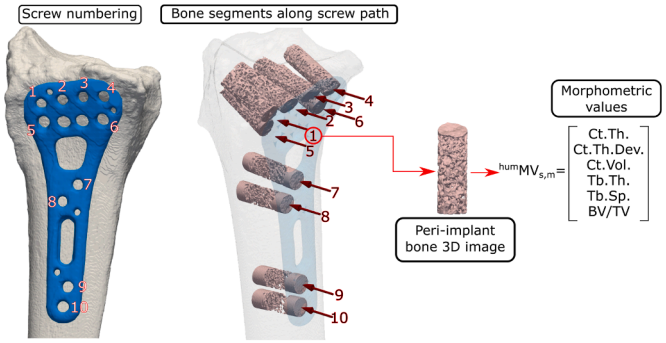

Fig. 2. Human bone analysis. Peri-implant bone morphometric values were calculated for 10 cylindrical volume of interests along the screw paths in 36 human radii CT images.

- Ct.Th.Dev.: Cortical thickness measurement deviation [mm]
- Ct.Vol.: Measured cortical volume [mm^3]
- BV/TV: Bone volume fraction, only calculated for the trabecular bone phase [-]
- Tb.Th.: Trabecular thickness [mm]
- Tb.Sp.: Trabecular spacing [mm]

Ct.Th., BV/TV, Tb.Th. and Th.Sp. were included in the calculation since they are among the standard set of cortical and trabecular structural parameters used to characterize bone structures [50]. It is also suggested there to report cortical area, but this was replaced by cortical volume in the present study in order to better differentiate between mono and bi cortical implantation. Cortical thickness measurement deviation, defined as the standard deviation of the measured cortical thickness using the method defined in [51], was selected to account for inhomogeneous cortical thickness (see Figure 3) and, thus, favour samples with uniform, "coin-shaped" cortical bone phases, similar to those observed in most peri-implant 3D images.

The recorded MVs of each peri-implant bone segment were then arranged in vector form as follows:

Fig. 3. Sample with uniform, "coin shaped", cortical section compared (A) compared to one with inhomogeneous cortical thickness (B). Cortical thickness measure deviation was used to favour probes similar (A) to the former and penalize (B).

$$ {}^{\text{hum}}\mathbf{MV}_{s,m} = \begin{bmatrix} \text{Ct.Th.} \\ \text{Ct.Th.Dev.} \\ \text{Ct.Vol.} \\ \text{Tb.Th.} \\ \text{Tb.Sp.} \\ \text{BV/TV} \end{bmatrix} \tag{1} $$

Where s represent the implantation site (1 to 10) and m represents each human radius (1 to 36) so, for example, ${}^{\text{hum}}\mathbf{MV}_{10,36}$ represents the peri-implant bone segment at the implantation site number 10 on the human radius number 36. By averaging the recorded ${}^{\text{hum}}\mathbf{MV}_{s,m}$ on each screw implantation site (1 to 10) across the 36 human radii, the MV vectors of 10 average implantation bone segments were calculated as follows:

$$ {}^{\text{target}}\overline{\mathbf{MV}}_{s} = \frac{1}{36}\sum_{m=1}^{36} {}^{\text{hum}}\mathbf{MV}_{s,m} \tag{2} $$

These average target bone segments, defined by their respective ${}^{\text{target}}\overline{\mathbf{MV}}_{s}$ vector, were then used as target values for the BoSS calculation.

2.2. Animal bone preparation

Four bones were harvested from each animal model: radius, humerus, tibia and femur. All bones were procured from slaughter age specimens (4-12 months for pig, 3-4 years for sheep) from local abattoirs in the state of Lower Austria. Soft tissue was carefully removed from each bone before placing a cut through the middle of the diaphysis thus isolating the proximal and distal fragments for the bone. Each fragment of bone and kept frozen at $-22^{\circ}C$ prior to CT scanning.

2.3. micro CT scanning and image processing

From each animal model, six bone regions were selected for scanning:

- Proximal and distal tibia
- Proximal and distal femur
- Proximal humerus
- Distal radius

scanning was performed in a micro-CT scanner (Bruker Skyscan 1173, Bruker Corp., Billerica MA, USA) using a voxel size of 0.076 *mm*, tube potential of 115 kVp and current of 30 μA. This voxel size was selected to match, as close as possible, that of the reference human scans. Cortical and trabecular bone phases were manually segmented from each bone using an open source slicing software (see www.slicer.org), which can be seen in Figure 4.

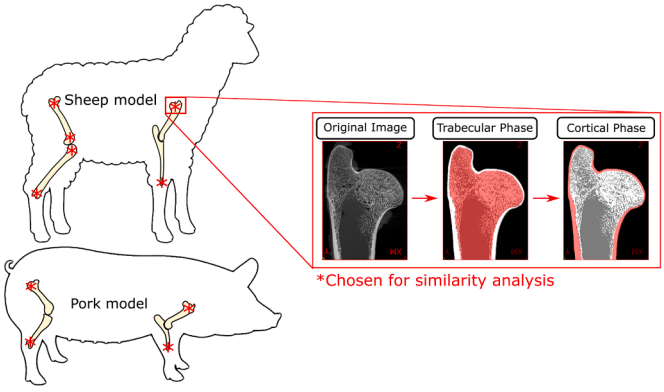

Fig. 4. Animal bones selected for analysis. For every bone, cortical and trabecular bone phases were segmented and analysed separately.

2.4. Computational approach for animal bone probing

Based on a surface mesh of each animal bone, a computational algorithm was designed to extract virtual cylinder probes on several locations covering the total triangulated bone surface from which the defined MVs were recorded. The exact location of these probes was set as the geometric centre point of each triangle on the surface mesh and oriented parallel to the normal vector of said triangle, this process can be seen in figure 5. The probe diameter was set to 4 *mm* (same as human samples) while the length was taken as the average screw implantation depth (14.6 2.76 *mm* with overall values ranging between 9.17 and 24.03 *mm*) calculated from the human CT scans. The number of triangles/probing points for each mesh ranged between 3000 and 4000. This value was chosen not only to preserve the bone geometry but also to have isometric triangles with an estimated edge length of ~ 2 *mm*.

For each proving point p, the local MVs were recorded and arranged in vector form as:

$$ {}^{\text{probe}}\mathbf{MV}_{p} = \begin{bmatrix} \text{Ct.Th.} \\ \text{Ct.Th.Dev.} \\ \text{Ct.Vol.} \\ \text{Tb.Th.} \\ \text{Tb.Sp.} \\ \text{BV/TV} \end{bmatrix} \tag{3} $$

2.5. Similarity score calculation

The definition of the bone similarity score (BoSS) begins by calculating the structural distance between the target bone segment (defined by equation 2) and each probe extracted from the animal models (defined by equation 3). Since both, target, and probe, are defined as vector expressions the calculated structural distance is also defined as vector whose individual components i correspond to:

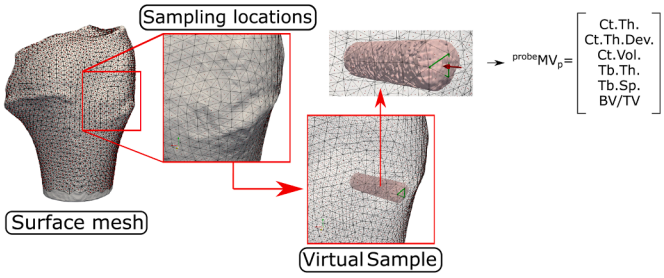

Fig. 5. Computational probing scheme. A virtual probe was placed on the center point of each triangle of an almost isometric ($\sim$2 *mm* edge length) surface mesh of each bone and the corresponding morphometric values were recorded.

$$^{probe}d_{s,p,i} = \frac{|^{target}\overline{MV}_{s,i} - {}^{probe}MV_{p,i}|}{^{target}\overline{MV}_{s,i}} \quad (4)$$

where $i = 1...6$ represents each component of the MV vector. So, for example, the BV/TV (i=6 in the MV vector) distance between the probed location 1000 and average target bone segment number 10 will be written as:

$$^{probe}d_{10,1000,6} \quad (5)$$

The BoSS is then defined as the inner product of the distance vector, $^{probe}\mathbf{d}_{s,p}$, with a weighting vector $\mathbf{f}$ as follows:

$$^{probe}BoSS_{s,p} = \mathbf{f}\cdot{}^{probe}\mathbf{d}_{s,p} \quad (6)$$

For the present study, all the weighting vector $\mathbf{f}$ components were set to 1.0.

2.6. Human bone bone similarity score

In order to better interpret the results following the method described above it was necessary to define a range of values that the BoSS can realistically have. this was done by comparing each peri-implant bone segment from each human radius ($^{hum}\mathbf{MV}_{s,m}$) with its corresponding target bone segment ($^{target}\overline{\mathbf{MV}}_{s}$) by modifying equations 6 and 4 to:

$$^{hum}d_{s,m,i} = \frac{|^{target}\overline{MV}_{s,i} - {}^{hum}MV_{s,m,i}|}{^{target}\overline{MV}_{s,i}} \quad (7)$$

Similar to the previous case, the BV/TV distance, between the average target bone segment at location 10 and the peri-implant bone segment extracted from radius 36 at the same location will be written as:

$$^{hum}d_{10,36,6} \quad (8)$$

The corresponding BoSS will then be:

$$^{hum}BoSS_{s,m} = \mathbf{f}\cdot{}^{hum}\mathbf{d}_{s,m} \quad (9)$$

This information was used to create a spectrum of human BoSS values which was then used to define thresholds for structural similarity between animal and human bone probes. Based on this it could be established whether a bone sample harvested from an animal model can be considered human-like based on its BoSS value and thus, kept for further mechanical testing.

2.7. Sample harvesting location based on BoSS

Based on the analysis on human radius samples presented in the previous subsection, the minimum $^{probe}BoSS_{s,p}$ location can be replaced by regions on the bone surface where samples with human-like BoSS values can be found. This representation can help overcome the following limitations of having a specific point for sample harvesting:

- Although possible, it is highly unlikely that two bones of the same type, e.g. pig distal radius, would present the exact minimum BoSS values in exactly the same location. This is problematic since most studies on orthopaedic implants need a large number of samples, which need to be harvested from more than one single bone.
- There is the possibility that a bone sample cannot be optimally (if at all) harvested from the resulting location of the minimum BoSS value.
- Even if the minimum BoSS location coincides between bones and a sample can be reliably harvested from said location, the computational time needed to individually analyse a large number of bones could be considerably high, all of which can make implementing this methodology impractical.

It will also be useful if these regions overlap among different bones. This would make it possible to define a consistent sample harvesting location based on a smaller number of individuals, even if the exact minimum $^{probe}BoSS_{s,p}$ location does not coincide across the studied bones. Based on this, two further pig distal radii were analysed in order to determine if overlapping regions with low $^{probe}BoSS_{s,p}$ values could be identified. The corresponding colour maps were modified to better display the sample harvesting regions where human-like samples are found. The bones were acquired from the same abattoir with one week between each acquisition thus guaranteeing different bone provenance. The idea behind this test was to determine if an ideal sample source location could be identified in the three specimens which will present similar BoSS values.

3. Results

A total of 420 surface colour maps, 70 for each one of the studied animal bones, were created with the methodology presented above (BoSS colour map plus seven specific distances per target bone segment). To avoid presenting repetitive information, the figures presented in this section correspond only to one animal model (pig proximal radius) unless the contrary is indicated. Despite of this, the information presented here is consistent among all animal bones with the figures only serving as visual aid for better interpreting the accompanying information. With this in mind, the following sections will then be dedicated to present the main results of this study following the general order defined in the methods section. All bones were analysed in a dedicated computing server (2x AMD EPIC 7551 CPUs with 32 Cores, 256 GB RAM) with average processing time for every animal bone ranging between 2 and 8 hours, depending on the bone size i.e., CT image size.

3.1. Human bone morphometric values

The calculated average target morphometric values can be seen in table 1.

Ct.Th., Ct.Th.Dev., Ct.Vol., and Tb.Sp. columns show that peri-implant bone segments number 1-6 have lower average values compared to 7-10. Conversely, the BV/TV column shows that the opposite happens for these same groups, i.e. peri-implant bone segments 1-6 show higher values. This information was useful for identifying

Table 1
Average morphometric values and their standard deviation averaged over the 36 human radii samples calculated for every screw implantation location. Every measured morphometric value showed variation with the anatomical location (proximal to distal) with the exception of trabecular thickness which remained mostly constant.

s	Ct.Th. [mm]	Ct.Th.Dev. [mm]	Ct.Vol. [mm^3]	BV/TV [-]	Tb.Th. [mm]	Tb.Sp. [mm]
1	0.45	0.10 0.05	5.45 2.06	0.21	0.29	0.89
	0.12			0.08	0.03	0.29
2	0.53	0.12 0.06	6.87 3.21	0.29	0.32	0.69
	0.19			0.08	0.04	0.10
3	0.46	0.10 0.03	6.35 3.08	0.29	0.31	0.68
	0.15			0.08	0.03	0.13
4	0.49	0.13 0.07	7.07 5.70	0.34	0.33	0.60
	0.19			0.09	0.03	0.10
5	0.72	0.14 0.05	9.98 3.97	0.22	0.29	0.80
	0.25			0.08	0.03	0.19
6	0.93	0.19 0.05	11.89 4.33	0.27	0.30	0.68
	0.32			0.08	0.02	0.16
7	1.54	0.29 0.08	39.87 9.53	0.13	0.29	1.38
	0.31			0.07	0.02	0.82
8	1.66	0.32 0.09	42.75	0.11	0.29	1.53
	0.35		10.48	0.06	0.02	0.86
9	2.00	0.41 0.10	54.53	0.06	0.28	2.26
	0.40		11.96	0.04	0.04	0.97
10	2.06	0.43 0.13	55.68	0.06	0.29	2.43
	0.43		13.09	0.04	0.05	0.97

which screws were implanted in the diaphyseal and epiphyseal regions of the bone indicating the type of implantation (that is, mono or bi cortical implantation). Average Tb.Th. appeared to be the same for all the peri-implant bone segments. Using this data the specific MV distances and bone similarity scores were calculated for every target bone segment, for all the scanned animal bones.

3.2. Animal bone morphometric distance and BoSS mapping

The specific structural distances ${}^{probe}d_{s,m,i}$ were recorded separately thus allowing to examine each one separately. This helps identify specific regions on a bone with desired morphological characteristics, for example low/high cortical thickness. An example of this mapping can be seen Figure 6.

For the purpose of this study, all MV distances were weighed equally (that is $\mathbf{f} = [1.0, 1.0, 1.0, 1.0, 1.0, 1.0]$) as mentioned before. Figure 7 shows the BoSS value mapping for target bone segment 1 on a pig distal radius as an example.

This mapping process was repeated for every target bone segment on every animal bone which allowed to locate the global minimum BoSS values for each one of the target bone segments among the tested bones. The location of the minimum ${}^{probe}BoSS_{s,p}$ values corresponds to the sample harvesting sites with the closes MV values to those of the peri-implant bone segments. These are shown in figure 8 with the location marked by an arrow.

Minimum ${}^{probe}BoSS_{s,p}$ values for target bone segment 1,4,7-9 were found on the pig distal femur, target bone segments 2, 3 and 6 were found on the pig proximal humerus and target bone segments 5 and 10 were found on the pig proximal femur and distal tibia, respectively.

3.3. BoSS calculation for human samples

In order to better interpret the results presented above it was necessary to define a reference bone similarity score spectrum which could in turn help determine high or low BoSS values. For this, the ${}^{hum}BoSS_{s,m}$ values for all peri-implant bone segments (s) across all human radii (m) was calculated as per equations 7 and 9. The ${}^{hum}BoSS_{s,m}$ value distributions for all peri-implant bone segments can be seen in figure 9.

Mean peri-implant ${}^{hum}BoSS_{s,m}$ values ranged between 1.46 and 3.05

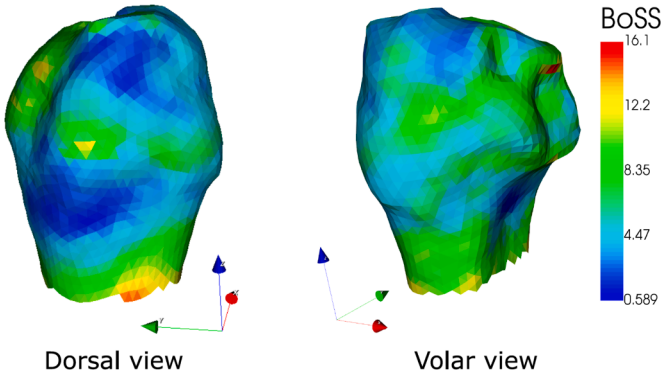

Fig. 7. Bone Similarity Score (${}^{probe}BoSS_{1,p}$) mapped to the bone surface for target bone segment number 1. Low BoSS value region, marked in blue, represent ideal sample harvesting locations for a particular target bone segment.

with overall values ranging between 0.26 and 18.5. The figure also shows that for every target bone segment the peri-implant ${}^{hum}BoSS_{s,m}$ values, meaning all the values between the minimum and maximum observations excluding outliers (whiskers), fall between 0 and 4. This allows to create a first BoSS category, i.e. "human-like" values. Furthermore, a considerable set of outliers fall between 4 and 10. While it is possible to separate these values between mild and extreme outliers, it is more convenient to group these values in a second category, "moderately human-like", allowing and treat these bone segments as a single group. Likewise, only three ${}^{hum}BoSS_{s,m}$ values were found above 10 which could be labelled "not human-like". Based on this, the defined categories for ${}^{hum}BoSS_{s,m}$ value ranking are:

- Human-like: ${}^{hum}BoSS_{s,m}$ values between 0 and 4, representing 93% of all peri-implant bone segments
- Moderately human-like: ${}^{hum}BoSS_{s,m}$ values between 4 and 10, representing 6% of all peri-implant bone segments
- Not human-like: ${}^{hum}BoSS_{s,m}$ values above 10, representing 1% of all peri-implant bone segments

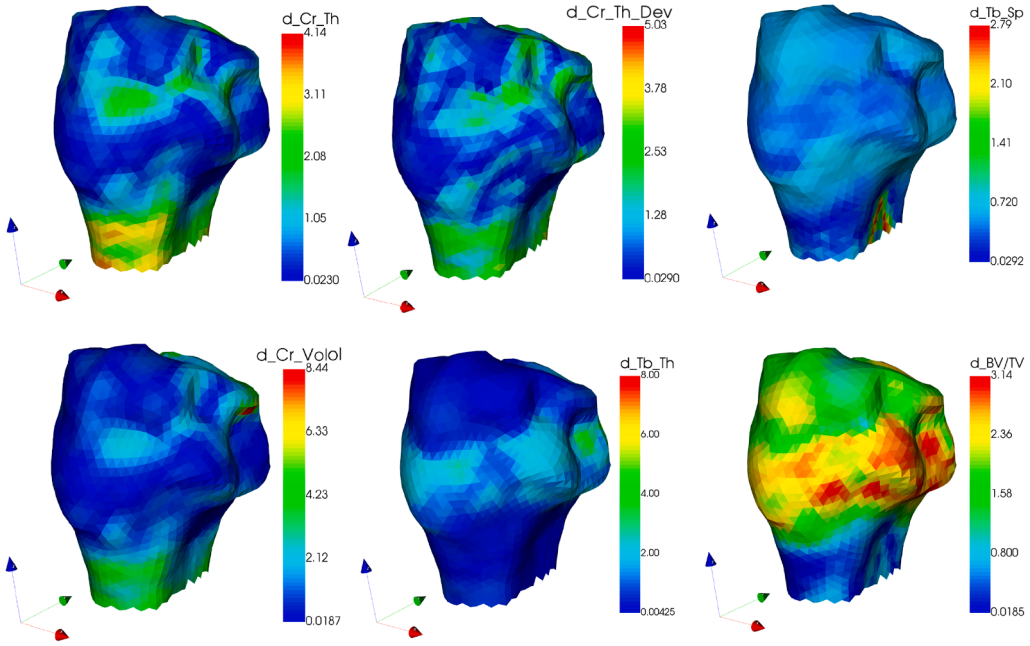

Fig. 6. Morphological distances (with "d" referring to ${}^{probe}d_{s,m,i}$) projected to the surface mesh of a pig distal radius for target screw number 1.

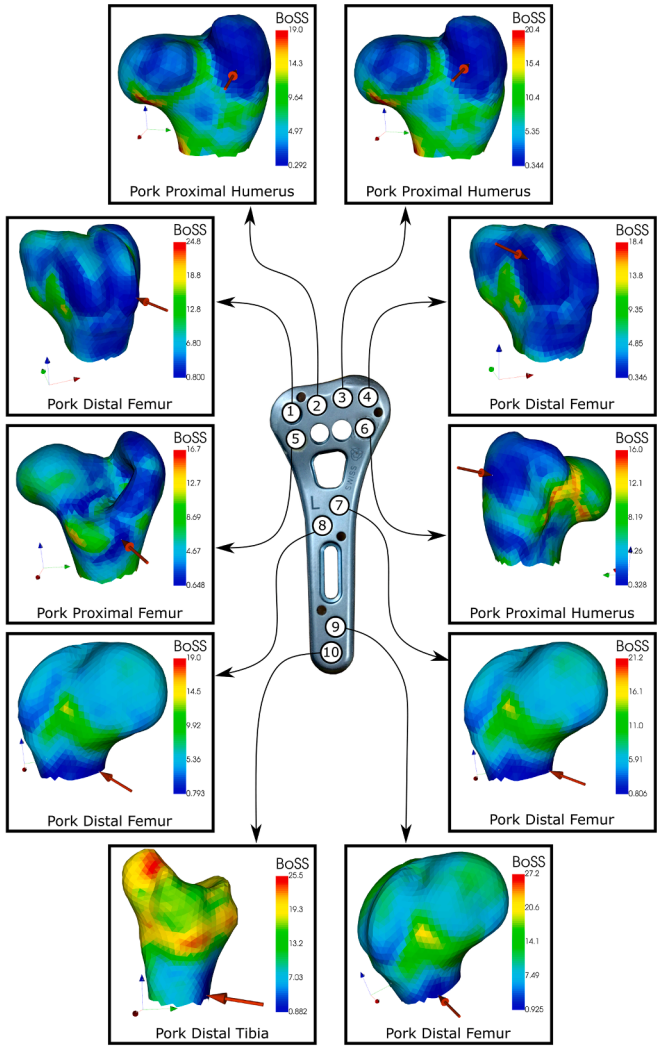

Fig. 8. Lowest $^{probe}BoSS_{s,p}$ locations for each target bone segment (1-10) found in the selected animal bone models marked on the surface of each bone with an arrow. For every target bone segment the lowest $^{probe}BoSS_{s,p}$ location was found on a pig bone, with most of them being found in the distal femur (5 target bone segments), followed by the proximal humerus (3) distal tibia (1) and proximal femur (1).

Figure 10 shows the probability density distributions of the grouped peri-implant bone segments $^{hum}BoSS_{s,m}$ values as well as a the "traffic light" system for sample segregation.

Based on this, the $^{probe}BoSS_{s,p}$ colour maps (figure 7) can be adjusted to better match the defined traffic light system, which is shown in figure 11.

3.4. BoSS for sample source selection

It is unlikely that two bones from different specimens will have the exact same number of probing location and moreover the exact $^{probe}BoSS_{s,p}$ values for every probe. Because of this, it was also of the interest of the study to evaluate whether bones with different provenance (meaning different specimens of the same species) would have similar $^{probe}BoSS_{s,p}$ values and colour maps. The results obtained after analysing two further pig distal radii are shown in Figure 12 which presents the colour maps, adjusted to fit the defined traffic light system, calculated for target bone segment 8 as an example.

While the specific minimum $^{probe}BoSS_{s,p}$ locations and value for every bone were not the same, the presented colour maps show qualitative

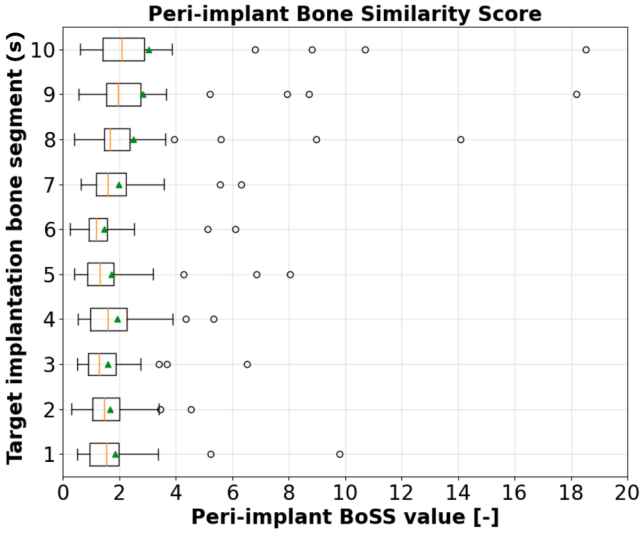

Fig. 9. Box and whiskers plot of the bone similarity score calculated for the human peri-implant bone segments. Mean values for each for are presented as green triangles.

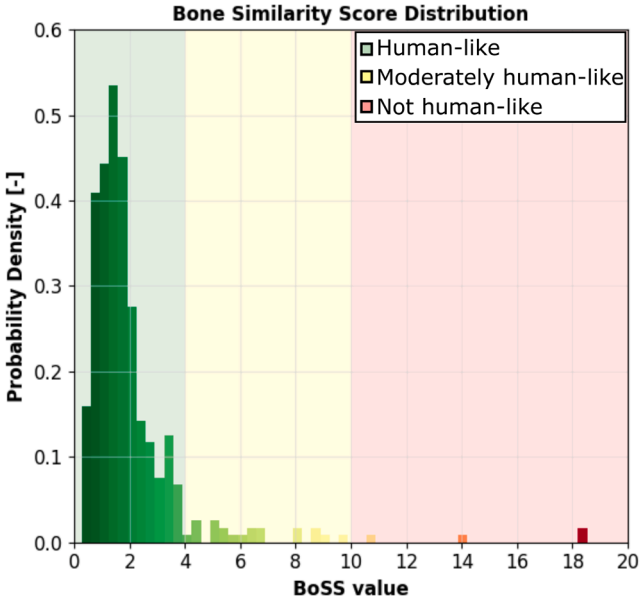

Fig. 10. Probability density distribution of the human peri-implant bone similarity score. A so-called traffic light system was used to categorize the values between an define acceptable BoSS value ranges for selecting animal bone sample sources.

similarity in addition to comparable $^{probe}BoSS_{s,p}$ value ranges which can be seen in Table 2.

4. Discussion

The purpose of this study was to develop a method for sample selection for screw mechanical testing on animal bones based on local bone morphometric values from real screw implantation sites. The proposed method could be used to identify regions in animal bones from where samples with "human-like" CT-derived morphology could be harvested and used for orthopaedic screw implantation and mechanical testing. A total of 360 virtual bone probes were extracted from 36 human radii [47,49] and used to quantify the average target bone morphometric values of ten real implantation sites. A computational algorithm

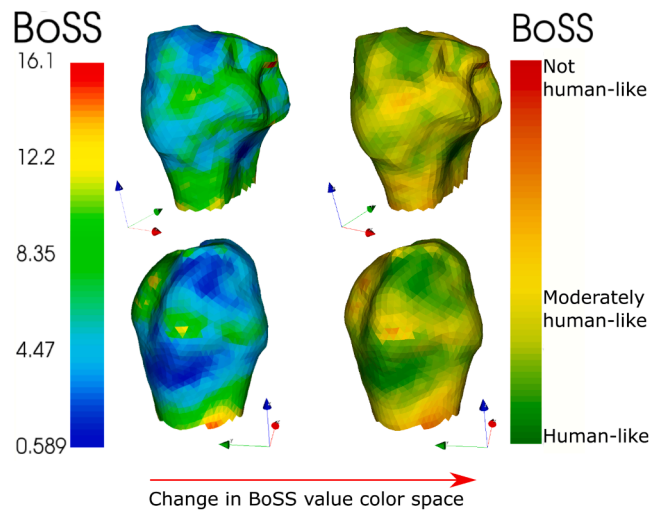

Fig. 11. Bone similarity score colour space remapped to the defined traffic light system.

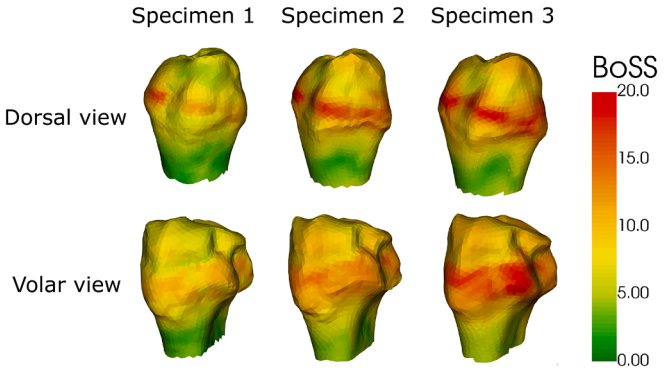

Fig. 12. Repetition tests done on a set of 3 pig distal radii for target bone segment number 8. Similar high/low BoSS value regions were found in common anatomical location across the three bones; the surface colour maps were adjusted to match the previously defined traffic light system.

Table 2
BoSS value ranges for every target bone segment for the three pig distal radii i.e. specimens 1-3. Across the three bones, BoSS value ranges were comparable for every target implantation bone segment.

	BoSS range		
s	Specimen 1	Specimen 2	Specimen 3
1	0.60-16.1	1.70-21.9	2.21-20.5
2	0.46-13.5	0.61-19.4	1.44-18.3
3	0.58-15.4	0.98-21.7	1.39-20.3
4	0.61-13.7	0.73-19.7	1.21-18.7
5	0.79-12.8	0.80-14.3	1.52-14.1
6	0.50-12.2	0.79-12.7	1.21-12.9
7	0.96-15.5	1.26-17.6	1.71-17.8
8	0.93-17.3	1.52-19.6	1.82-19.7
9	1.64-22.1	1.47-25.2	1.60-25.4
10	1.27-22.5	1.27-25.6	1.44-25.8

was then created to extract a large number of virtual probes from an animal bone and compare the corresponding local CT-MVs with the calculated average peri-implant values resulting in a bone similarity score, BoSS for short. This information was then used to identify regions in animal bones with low BoSS values which could be used to identify sample harvesting locations for orthopaedic screw testing. The following sections will discuss the results presented above.

4.1. Human bone morphometric analysis

The human bone morphometric values calculated here are comparable to those presented in [46], where the morphometric indices from 100 human distal radii with a comparable donor age (average age (years): men 79.7, women 81.5) to that of the patients of this study (82.4 years) were recorded using a different approach, that is whole bone instead of screw implantation site. Cortical thickness, trabecular bone volume fraction and trabecular spacing showed comparable overall values in both studies with the recorded values being dependent on the anatomical position, that means higher Ct.Th. and Tb.Sp. in more proximal regions of the bone with the opposite trend observed for BV/TV. While overall trabecular thickness values in both studies were comparable, the reported increase in trabecular thickness from the distal to proximal end of the bone was not observed in this study, as it was already mentioned before.

4.2. Structural distance and BoSS value mapping

The structural distance maps (Figure 6) show that specific CT-MVs from older individuals can be accurately located in large portions of the animal bones following the methodology presented here. This seems to contradict the results presented by other authors where animal bones, particularly pig and bovine bones, are better suited to replace those of young athletic humans [11,36] since older patient tend to have degraded bone architecture due to bone degenerative diseases. By combining the specific morphometric values in a multi-parametric similarity score it can be seen how the structurally similar regions considerably narrow down (figure 7). This accurately reflects the aforementioned results and also demonstrates that some specific locations on a young animal bone could serve as sample sources for osteoporotic bone analogues; this is further depicted in Figure 8 were all the average target bone segments are located in animal bones with high structural similarity.

4.3. BoSS based sample selection for screw testing

To the best of our knowledge, there is no defined methodology or protocol for animal bone sample source selection based on multi-parametric characterization of local bone morphology. By studying the inter subject variability of the BoSS score (figure 12) it was shown that the BoSS value distributions among different subjects can indeed be compared, thus allowing the selection of a consistent sample harvesting site on the bone where the structural distance to a human sample will be, ideally, minimum. This result is particularly interesting because, even if the specific BoSS values are not the same, the selected regions still represent acceptable matches found on a specific bone and they overlap among several bones. Despite this, a broader study with more test subjects is highly recommended in order to fully determine if BoSS mapping is consistent among several individuals.

4.4. Guidelines for bone surrogate sample selection for orthopaedic screw testing

As mentioned in [42], a major setback for the presented methodology is the lack of BoSS value threshold or limit value which could help determine whether an animal sample is indeed structurally similar to a human bone. An attempt to overcome this problem is presented here by calculating a bone similarity score for virtual human samples. Figure 9 indicates that most of the harvested human samples with a ${}^{\text{hum}}BoSS_{s,m}$ value between 1 and 4 will fall into a sort of "human-like" category which can be further observed in figure 10, were two further categories, moderately human-like and not human-like are defined. Using this information, an alternative path to sample selection can be drawn as follows:

1. A small number of bones is fully analysed in order to identify ideal sample harvesting locations from which a larger number of samples will be harvested
2. All the harvested samples are scanned and the respective BoSS values are calculated
3. Based on the BoSS values, the samples are categorised (human-like, moderately human-like or not human-like) and either discarded or kept for further testing

A graphical schematic of these steps can be seen in 13.

As it has been pointed out before, the underlying bone morphology where a screw is implanted has an effect on its mechanical competence [6,7,9]. By following the steps presented above, this methodology allows to test orthopaedic screws intended for human bones in samples harvested from animal bones. This makes it possible to test the influence of the human bone architecture on the holding capacity of an implanted bone screw while at the same time avoiding the shortcomings of conducting mechanical test on human bones and synthetic bone analogues.

4.5. Limitations

The main drawback from this study is that it is not known if two samples with similar bone similarity score values have similar mechanical properties. As pointed out before, some underlying bone morphometric values, such as cortical thickness and bone volume fraction, correlate well with the screw holding capacity this, however, needs to be further confirmed experimentally.

Another major drawback from the sample selection approach presented here is the extensive computational cost associated with this analysis. This issue could be improved by optimizing the implemented scripts or using a more efficient programming language such as FORTRAN or C++. A different approach to reduce the computational cost is to reduce the number of probing points by using a coarser mesh. By reducing the mesh size by ~ 40 percent the computational time is proportionally reduce without compromising either the geometric representation of the bone or the BoSS mapping onto the bone surface. furthermore, it might not be necessary to analyse a whole bone if its already known that certain regions (the articular surface, for example) are not suitable for screw implantation. By analysing only a section of the bone, in combination with a coarse mesh, the computation time can be cut to under 1 hour.

That being said, without a dedicated computing server it might not be possible to conduct a study using this approach with a high mesh resolution.

Another limitation, as pointed in both [42] and [45] is related to the weighting of the individual morphometric values (**f**). For the present study 6 individual structural indices were selected but there was not a rigorous study of which ones were more determinant, especially in the context of mechanical testing. It is somehow evident that parameters like cortical thickness and bone volume fraction have a direct effect on the mechanical properties of the bone samples but the same cannot be said of cortical thickness measure deviation or trabecular spacing. A more rigorous quantification of the impact of each individual factor is then strongly advised. Furthermore, as mentioned in the discussion section, the suggested path for sample selection is based on the analysis of only three bones. Despite the obtained results being satisfactory for the purposes of this study, it is necessary to increase the sample size for confirmation.

Finally, it is worth mentioning that probing depth can also have an impact on the calculated bone similarity scores. For the present study, the probing depth was kept constant and equal to the average screw insertion depth in order to decrease the overall computational cost. The problem with doing this is that it is assumed that the average insertion depth of every peri-implant bone segment is the same which is not the case. A further study where the influence of the insertion depth of each individual peri-implant bone segment is then advised in order to determine if this should be considered or not.

5. Conclusions

The methodology presented here provides a procedure for bone surrogate sample selection which is not known to be previously reported. The results presented here allow to conclude that human-like bone samples can be found in any of the analysed animal bones by

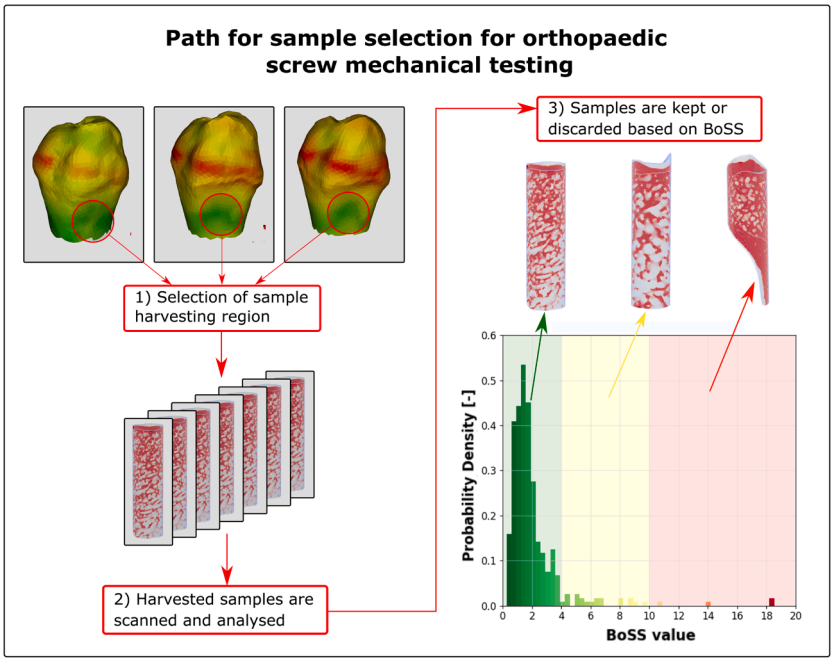

Fig. 13. Proposed path for sample selection. (1) A common region with known low BoSS values is selected for sample harvesting. (2) The harvested samples are scanned and analysed, that is, the morphometric distances and bone similarity score is calculated. Based on the latter, (3) the samples are either discarded or kept for further mechanical testing.

quantifying the local bone morphology. The described methods can be easily replicated, given the availability of the required computational power, and it relies on well-established image processing methods. Furthermore, this approach can be expanded to cover more screw types and other screw-like orthopaedic implants which reduces the need for testing human bones and the associated drawbacks of doing it. In the future, this sample selection method could be of considerable advantage for biomechanical studies, especially if human tissue is limited or not available for being studied.

Disclosure of conflicts of interest

The following additional information is required for submission. Please note that this form runs over two pages and failure to respond to these questions/statements will mean your submission will be returned to you. If you have nothing to declare in any of these categories then this should be stated

CRediT authorship contribution statement

J.D. Silva-Henao: Methodology, Software, Validation, Formal analysis, Investigation, Data curation, Writing – original draft, Funding acquisition. **A. Synek:** Investigation, Data curation, Writing – review & editing. **D.H. Pahr:** Resources, Project administration, Funding acquisition, Supervision, Writing – review & editing. **A.G. Reisinger:** Conceptualization, Resources, Project administration, Funding acquisition, Supervision, Writing – review & editing.

Acknowledgements

The authors declare no conflict of interest related to this study. This project was funded by the Gesellschaft fr Forschungsfrderung Niedersterreich m.b.H. Life Science Call 2017 Grant No. LS17-004 and Science call 2019 Dissertationen Grant No. SC19-014. No ethical approval was required for this study.

References

[1] Soong M, Van Leerdam R, Guitton TG, Got C, Katarincic J, Ring D. Fracture of the distal radius: risk factors for complications after locked volar plate fixation. J Hand Surg 2011. https://doi.org/10.1016/j.jhsa.2010.09.033.

[2] Nakashima H, Yukawa Y, Imagama S, Tokumi K, Kamiya M, Yanase M, Ito K, Machino M, Yoshida G, Ishikawa Y, Matsuyama Y, Ishiguro N, Kato F. Complications of cervical pedicle screw fixation for nontraumatic lesions: a multicenter study of 84 patients - Clinical article. J Neurosur: Spine 2012. https://doi.org/10.3171/2011.11.SPINE11102.

[3] Deen HG, Nottmeier EW, Reimer R. Early complications of posterior rod-screw fixation of the cervical and upper thoracic spine. Neurosurgery 2006. https://doi.org/10.1227/01.neu.0000245592.54204.d0.

[4] Arora R, Lutz M, Hennerbichler A, Krappinger D, Espen D, Gabl M. Complications following internal fixation of unstable distal radius fracture with a palmar locking-plate. J Orthopaed Trauma 2007. https://doi.org/10.1097/BOT.0b013e318059b993.

[5] Esses SI, Sachs BL, Dreyzin V. Complications associated with the technique of pedicle screw fixation: a selected survey of abs members. Spine 1993. https://doi.org/10.1097/00007632-199311000-00015.

[6] Wirth AJ, Mueller TL, Vereecken W, Flaig C, Arbenz P, Müller R, Van Lenthe GH. Mechanical competence of bone-implant systems can accurately be determined by image-based micro-finite element analyses. Arch Appl Mech 2010. https://doi.org/10.1007/s00419-009-0387-x.

[7] Basler SE, Traxler J, Müller R, van Lenthe GH. Peri-implant bone microstructure determines dynamic implant cut-out. Med Eng Phys 2013. https://doi.org/10.1016/j.medengphy.2013.03.016.

[8] Varga P, Grünwald L, Windolf M. The prediction of cyclic proximal humerus fracture fixation failure by various bone density measures. J Orthopaed Res 2018. https://doi.org/10.1002/jor.23879.

[9] Seebeck J, Goldhahn J, Städele H, Messmer P, Morlock MM, Schneider E. Effect of cortical thickness and cancellous bone density on the holding strength of internal fixator screws. J Orthopaed Res 2004. https://doi.org/10.1016/j.orthres.2004.04.001.

[10] Akbay A, Bozkurt G, Ilgaz O, Palaoglu S, Akalan N, Benzel EC. A demineralized calf vertebra model as an alternative to classic osteoporotic vertebra models for pedicle screw pullout studies. Eur Spine J 2008. https://doi.org/10.1007/s00586-007-0545-1.

[11] Fletcher JW, Williams S, Whitehouse MR, Gill HS, Preatoni E. Juvenile bovine bone is an appropriate surrogate for normal and reduced density human bone in biomechanical testing: a validation study. Sci Rep 2018. https://doi.org/10.1038/s41598-018-28155-w.

[12] Patel PS, Shepherd DE, Hukins DW. Compressive properties of commercially available polyurethane foams as mechanical models for osteoporotic human cancellous bone. BMC Musculoskeletal Disord 2008;9:1–7. https://doi.org/10.1186/1471-2474-9-137/TABLES/2.https://www.bmcmusculoskeletdisord.biomedcentral.com/articles/10.1186/1471-2474-9-137

[13] Johnson AE, Keller TS. Mechanical properties of open-cell foam synthetic thoracic vertebrae. J Mater Sci Mater Med 2008;19:1317–23. https://doi.org/10.1007/S10856-007-3158-7.https://pubmed.ncbi.nlm.nih.gov/17882383/

[14] Shen F, Kim HJ, Kang KT, Yeom JS. Comparison of the pullout strength of pedicle screws according to the thread design for various degrees of bone quality. Appl Sci 2019, Vol 9, Page 1525 2019;9:1525. https://doi.org/10.3390/APP9081525.https://www.mdpi.com/2076-3417/9/8/1525/htmhttps://www.mdpi.com/2076-3417/9/8/1525

[15] Erhart J, Unger E, Trulson I, Hagmann M, Ristl R, Trulson A, Hajdu S, Schefzig P, Gormasz A, Mayr W. Pull-out forces of headless compression screws in variations of synthetic bone models imitating different types of scaphoid fractures in good bone quality. J Mater Sci: Mater Med 2020;31:1–11. https://doi.org/10.1007/S10856-020-06445-Y/TABLES/6.https://link.springer.com/article/10.1007/s10856-020-06445-y

[16] Pan CY, Chou ST, Tseng YC, Yang YH, Wu CY, Lan TH, Liu PH, Chang HP. Influence of different implant materials on the primary stability of orthodontic mini-implants. Kaohsiung J Med Sci 2012;28:673–8. https://doi.org/10.1016/J.KJMS.2012.04.037.https://pubmed.ncbi.nlm.nih.gov/23217360/

[17] Moser JE, Kunkel KA, Gerard PD. Pullout strength of 2.0 mm cancellous and cortical screws in synthetic bone. Veterin Surg: VS 2017;46:1110–5. https://doi.org/10.1111/VSU.12692.https://pubmed.ncbi.nlm.nih.gov/28817191/

[18] Palissery V, Taylor M, Browne M. Fatigue characterization of a polymer foam to use as a cancellous bone analog material in the assessment of orthopaedic devices. J Mater Sci Mater Med 2004;15:61–7. https://doi.org/10.1023/B:JMSM.0000010098.65572.3B.https://pubmed.ncbi.nlm.nih.gov/15338592/

[19] Muhayudin NA, Basaruddin KS, McEvoy F, Tansey A. Evaluating compressive properties and morphology of expandable polyurethane foam for use in a synthetic paediatric spine. J Mater Res Technol 2020;9:2590–7. https://doi.org/10.1016/J.JMRT.2019.12.089.

[20] Wancket LM. Animal Models for Evaluation of Bone Implants and Devices: comparative Bone Structure and Common Model Uses. Vet Pathol 2015. https://doi.org/10.1177/0300985815593124.

[21] Pearce A.I., Richards R.G., Milz S., Schneider E., Pearce S.G.. Animal models for implant biomaterial research in bone: a review. 2007. 10.22203/eCM.v013a01.

[22] Gabriele Sommer N, Hahn D, Okutan B, Marek R, Weinberg A-M. Animal models in orthopedic research: the proper animal model to answer fundamental questions on bone healing depending on pathology and implant material. Animal Models in Medicine and Biology. 2020. https://doi.org/10.5772/intechopen.89137.

[23] Kanayama M, Cunningham BW, Weis JC, Parker LM, Kaneda K, McAfee PC. Maturation of the posterolateral spinal fusion and its effect on load- sharing of spinal instrumentation. J Bone Joint Surg - Ser A 1997. https://doi.org/10.2106/00004623-199711000-00013.

[24] Yaman O, Demir T, Arslan AK, Iyidiker MA, Tolunay T, Camuscu N, Ulutas M. The comparison of pullout strengths of various pedicle screw designs on synthetic foams and ovine vertebrae. Turkish Neurosurg 2015. https://doi.org/10.5137/1019-5149.JTN.8907-13.1.

[25] Tolunay T, Bagül C, Demir T, Yaman ME, Arslan AK. Pullout performance comparison of pedicle screws based on cement application and design parameters. Proc Inst Mech Eng, Part H: J Eng Med 2015. https://doi.org/10.1177/0954411915612494.

[26] Aycan MF, Yaman ME, Usta Y, Demir T, Tolunay T. Investigation of toggling effect on pullout performance of pedicle screws. Proc Inst Mech Eng H 2018. https://doi.org/10.1177/0954411918755417.

[27] Zou X, Li H, Teng X, Xue Q, Egund N, Lind M, Bünger C. Pedicle screw fixation enhances anterior lumbar interbody fusion with porous tantalum cages: an experimental study in pigs. Spine 2005. https://doi.org/10.1097/01.brs.0000170588.80377.3f.

[28] Carvalho PH, Saavedra MdSF, Ballester RY, Luz JGC. Biomechanical evaluation of the sheep mandible as a model for studying fixation methods. Int J Morphol 2018. https://doi.org/10.4067/S0717-95022018000300926.

[29] Mueller CK, Solcher P, Peisker A, Mtsariashvilli M, Schlegel KA, Hildebrand G, Rost J, Liefeith K, Chen J, Schultze-Mosgau S. Analysis of the influence of the macro- and microstructure of dental zirconium implants on osseointegration: A minipig study. Oral Surg Oral Med Oral Pathol Oral Radiol 2013. https://doi.org/10.1016/j.oooo.2011.10.041.

[30] Schaller B, Saulacic N, Beck S, Imwinkelried T, Goh BT, Nakahara K, Hofstetter W, Iizuka T. In vivo degradation of a new concept of magnesium-based rivet-screws in the minipig mandibular bone. Mater Sci Eng C 2016. https://doi.org/10.1016/j.msec.2016.06.085.

[31] He X, Reichl FX, Milz S, Michalke B, Wu X, Sprecher CM, Yang Y, Gahlert M, Röhling S, Kniha H, Hickel R, Högg C. Titanium and zirconium release from titanium- and zirconia implants in mini pig maxillae and their toxicity in vitro. Dental Mater 2020. https://doi.org/10.1016/j.dental.2020.01.013.

[32] Johnson TB, Siderits B, Nye S, Jeong YH, Han SH, Rhyu IC, Han JS, Deguchi T, Beck FM, Kim DG. Effect of guided bone regeneration on bone quality surrounding dental implants. J Biomech 2018. https://doi.org/10.1016/j.jbiomech.2018.08.011.

[33] Voumard B, Maquer G, Heuberger P, Zysset PK, Wolfram U. Peroperative estimation of bone quality and primary dental implant stability. J Mech Behav Biomed Mater 2019. https://doi.org/10.1016/j.jmbbm.2018.12.035.
[34] Assad-Loss TF, Kitahara-Céia FMF, Silveira GS, Elias CN, Mucha JN. Fracture strength of orthodontic mini-implants. Dental Press J Orthodontic 2017. https://doi.org/10.1590/2177-6709.22.3.047-054.oar.
[35] Pithon MM, Figueiredo DSF, Oliveira DD. Mechanical evaluation of orthodontic mini-implants of different lengths. J Oral Maxillofac Surg 2013. https://doi.org/10.1016/j.joms.2012.10.002.
[36] Lenz M, Gueorguiev B, Garces JB, Swords MP, Rammelt S, Hofmann GO, Zderic I, Ernst M, Richards RG, Sands AK. Axial and shear pullout forces of composite, porcine and human metatarsal and cuboid bones. J Orthopaed Transl 2018. https://doi.org/10.1016/j.jot.2018.06.001.
[37] Ayzenberg M, Arango D, Gershkovich GE, Samuel PS, Saing M. Pullout strength of a novel hybrid fixation technique (Tape Locking Screw) in soft-tissue ACL reconstruction: a biomechanical study in human and porcine bone. Orthopaed Traumatol: Surg Res 2017. https://doi.org/10.1016/j.otsr.2017.01.006.
[38] Christensen J, Fischer B, Nute M, Rizza R. Fixation Strength of Polyetheretherketone Sheath-and-Bullet Device for Soft Tissue Repair in the Foot and Ankle. J Foot Ankle Surg 2018. https://doi.org/10.1053/j.jfas.2017.08.004.
[39] Harper RA, Pfeiffer FM, Choma TJ. The minipig as a potential model for pedicle screw fixation: morphometry and mechanics. J Orthopaed Surg Res 2019. https://doi.org/10.1186/s13018-019-1292-9.
[40] Gifty T, Maksym P, Ihtesham R, Gwendolen R. A 3-dimensional biomimetic in-vitro bone model for testing small orthopaedic implants. Front Bioeng Biotechnol 2016. https://doi.org/10.3389/conf.fbioe.2016.01.01432.
[41] Egermann M, Goldhahn J, Schneider E. Animal models for fracture treatment in osteoporosis. Osteoporosis International. 2005. https://doi.org/10.1007/s00198-005-1859-7.
[42] Falvo D'Urso Labate G, Baino F, Terzini M, Audenino A, Vitale-Brovarone C, Segers P, Quarto R, Catapano G. Bone structural similarity score: a multiparametric tool to match properties of biomimetic bone substitutes with their target tissues. J Appl Biomater Funct Mater 2016. https://doi.org/10.5301/jabfm.5000283.
[43] Falvo D'Urso Labate G, Catapano G, Vitale-Brovarone C, Baino F. Quantifying the micro-architectural similarity of bioceramic scaffolds to bone. Ceramic Int 2017. https://doi.org/10.1016/j.ceramint.2017.04.121.
[44] Van Cleynenbreugel T, Schrooten J, Van Oosterwyck H, Vander Sloten J. Micro-CT-based screening of biomechanical and structural properties of bone tissue engineering scaffolds. Med Biol Eng Comput 2006. https://doi.org/10.1007/s11517-006-0071-z.
[45] Estermann SJ, Pahr DH, Reisinger A. Quantifying tactile properties of liver tissue, silicone elastomers, and a 3D printed polymer for manufacturing realistic organ models. J Mech Behav Biomed Mater 2020. https://doi.org/10.1016/j.jmbbm.2020.103630.
[46] Mueller TL, van Lenthe GH, Stauber M, Gratzke C, Eckstein F, Müller R. Regional, age and gender differences in architectural measures of bone quality and their correlation to bone mechanical competence in the human radius of an elderly population. Bone 2009. https://doi.org/10.1016/j.bone.2009.06.031.
[47] Synek A, Chevalier Y, Baumbach SF, Pahr DH. The influence of bone density and anisotropy in finite element models of distal radius fracture osteosynthesis: evaluations and comparison to experiments. J Biomech 2015. https://doi.org/10.1016/j.jbiomech.2015.10.012.
[48] Schiuma D, Brianza S, Tami AE. Development of a novel method for surgical implant design optimization through noninvasive assessment of local bone properties. Med Eng Phys 2011. https://doi.org/10.1016/j.medengphy.2010.09.024.
[49] Synek A. A specimen specific finite element validation study of distal radius fracture osteosynthesis. Technische Universität Wien; 2015. Diploma thesis. http://hdl.handle.net/20.500.12708/5151
[50] Bouxsein M.L., Boyd S.K., Christiansen B.A., Guldberg R.E., Jepsen K.J., Müller R.. Guidelines for assessment of bone microstructure in rodents using micro-computed tomography. 2010. 10.1002/jbmr.141.
[51] Hildebrand T, Rüegsegger P. A new method for the model-independent assessment of thickness in three-dimensional images. J Microsc 1997. https://doi.org/10.1046/j.1365-2818.1997.1340694.x.